Contrast-enhanced Ultrasound in the Assessment of the Transitional Zone of Microwave Ablations in an *Ex vivo* Perfused Liver Model; is It a Useful Tool?

Ahmed Alzaraa[1*], Wen Yuan Chung[1], Bruno Morgan[2], Kevin West[3] and David Lloyd[1]

[1]*Department of Hepatobiliary and Pancreatic Surgery, University Hospitals of Leicester, Leicester General Hospital, Leicester, LE5 4PW, United Kingdom.*
[2]*Department of Radiology, University Hospitals of Leicester, Leicester General Hospital, Leicester, LE5 4PW, United Kingdom.*
[3]*Department of Histopathology, University Hospitals of Leicester, Leicester General Hospital, Leicester, LE5 4PW, United Kingdom.*

Authors' contributions

This work was carried out in collaboration between all authors. Author AA; principal investigator, did the experiments and wrote the article, author WYC assisted in the experiments, author BM interepreted radiology images, author KW interepreted histology slides, author DL supervised the project and edited the article. All authors read and approved the final manuscript.

ABSTRACT

Background and Aims: Microwave ablation (MWA) under different imaging guidance is a new technique for treating liver malignancies. The ablation creates a transitional zone at the periphery of the ablated region. In this zone, few cancer cells might escape heat causing local recurrence. Therefore, a more defined transitional zone is required to avoid residual cancer.
Study Design: Experimental study with a block design.
Place and Duration of Study: Departments of Hepatobiliary and Pancreatic surgery, department of Radiology and department of Histopathology; University hospitals of Leicester, UK. May-July

---

Corresponding author: Email: ahmedwahabf@googlemail.com;

2011.

Methodology: MWA with different powers (50 W, 70 W, 90 W) were created in five ex vivo perfused porcine livers. The ablations were evaluated on morphology, grey-scale US, CEUS and histology. Statistical analysis of the data was performed using ANOVA test.

Results: CEUS showed better demarcation of the lesion's border when compared with the grey-scale US. There was a significant difference in the long axis of the ablation among morphology, grey-scale US and CEUS (P < 0.0001), and a significant difference in the lesion size between powers (P = 0.0064). There was no difference in the short-axis, but a significant difference in the lesion size between powers (P = 0.0306). A significant difference in the width of the transitional zone (TZ) was noticed between powers 50W and 90W (P= 0.015).

Conclusion: CEUS shows better demarcation of the ablated zone when compared with the grey-scale-US, a finding that could provide guidance in the assessment of the ablation zone during treatment. CEUS does not show superiority over morphology or grey-scale US in reflecting the actual size of the lesion. Histology remains the only method to provide exact measurements of the transitional zone width when compared with morphology. Further research is required to confirm these results.

Keywords: Microwaves; ablation; liver; contrast.

ABBREVIATIONS

Microwave ablations (MWA); Contrast-enhanced ultrasound (CEUS); ultrasound (US); transitional zone (TZ); computerised tomography (CT); magnetic resonance imaging (MRI); portal vein (PV); hepatic artery (HA); inferior vena cava (IVC); contrast agent (CA); long axis (LA); short axis (SA); Haematoxylin-Eosin (HE); hepatocellular carcinoma (HCC); radiofrequency ablation (RFA); contrast-enhanced intraoperative ultrasound (CE-IOUS).

1. INTRODUCTION

MWA is one of the new developing trends for treating cancer. Its mechanism of action is based on heat generation by inserting an applicator "connected to a microwave generator" into tumours [1,2]. The emitted electromagnetic waves cause friction movements of water molecules which generate heat ranging from 900 MHZ to 2500 MHz [1,3-5]. The heat is evenly conducted throughout the surrounding tissues around the applicator resulting in a spherical thermocoagulation zone [1,6,7]. Like with other trends of thermal ablation, although to a lesser extent, the generated heat with MWA can cause charring of the central tissue around the probe, especially with high power and long duration [8]. This carbonated layer acts as a barrier to heat conduction to the surrounding zones mainly at the periphery, an area called transitional zone (TZ) [2]. This is the zone where few cancer cells might escape heat leaving behind a residual tumour which consequently causes local recurrence. After ablation, the reactive tissue inflammation is shown as a hyperaemic rim surrounding the ablated zone [9,12]. This rim makes it difficult to differentiate between complete ablation and residual tumour [9-13].

The rim is not visible on grey-scale US, but with contrast (CT, MRI, CEUS), it is shown as uniform in thickness in benign lesions and irregular if residual tumour is still present in the ablated lesion [11,13]. Hence, immediate evaluation of the ablated zone is required to achieve complete lesion destruction in situ [13,14].

Different *in vivo* and *ex vivo* experimental and clinical studies have been performed to evaluate the relation between power, type of probe and ablation size on morphology, histology, and radiology. Gravante G and colleagues concluded that the correct use of MWA with technical improvement in the equipment could achieve a large ablation size with a high rate of complete tumour destruction [15]. That conclusion was also confirmed by four more studies [5,8,16,17]. Other experiments assessed ablation lesions on morphology, histology and imaging. Matsukawa, et al. [18] compared the created MWA lesions in 12 cadaveric porcine livers and 9 live rabbit livers on histology and grey-scale US. He found that the hyperechoic areas measured with grey-scale US were significantly larger than the actual necrotic areas (p < 0.01) on histology, probably due to air bubbles which developed within the tissue. Correlation between histology and MRI intensity signal (low in the central necrotic zone,

a high in the intermediate zone and an isointensity in the outer zone) was demonstrated in other studies [19,20]. CT showed a hypodense necrotic ablated lesion with no enhancement with contrast [17,19,21]. Lesion evaluation with these methods has few practical and logistical issues such as efficiency of the imaging technique, exposure to radiation, cost, time, experimenting on live animals and the need for a well-trained radiographer or surgeon with enough knowledge to assess targeted lesion during or after treatment [22,23].

Hypothesis: In this study, we wanted to find out whether the use of contrast-enhanced ultrasound (CEUS) would provide better assessment of the transitional zone of the MWA in an ex vivo perfused porcine liver model.

2. MATERIALS AND METHODS

2.1 Liver Procurement

Five white pigs weighing between 45 and 60 kg (already being killed for consumption) were humanely sacrificed in accordance to the Home Office regulations. A pre-heparinised non-pyogenic container with 5000 Units of Heparin was used to collect the autologous blood. The livers were then retrieved with a minimal warm ischemic time and two litres of cold Soltran solution (Baxter Healthcare, Thetford, United Kingdom) were perfused, one litre into the portal vein (PV) and one litre into the hepatic artery (HA). After the cold perfusion, the liver was transported on ice from the abattoir to the laboratory.

2.2 Circuit Preparation

The autologous heparinised blood was used to prime the circuit during the backbench preparation. Cannulation of the PV, HA, bile duct, supra- and infra-hepatic inferior vena cava (IVC) was carried out during the priming. Before connecting the liver to the circuit, 1 litre of 0.9% Normal Saline solution (Baxter Healthcare, Thetford, United Kingdom) was perfused through the PV and HA to flush out the Soltran solution and remove air from the organ and the cannulae. The liver was then placed in a non-pyogenic perfusion container and connected to the extracorporeal circuit.

2.3 Perfusion

The extracorporeal circuit (Medtronic Inc., Minneapolis, Minnesota - United States) consisted of an automatic centrifugal pump which provided the hepatic arterial flow and pressure, an oxygenator, a heat exchanger unit and a blood reservoir to simulate the venous flow and pressure (Fig. 1). The venous blood was collected from the supra- and infra-hepatic IVC and returned to the centrifugal pump. Parenteral nutrition, vasodilating prostacyclins, sodium bicarbonate, sodium taurocholate and insulin were added to the circulation to optimise the physiological condition of the system. Perfusion was carried out for six hours.
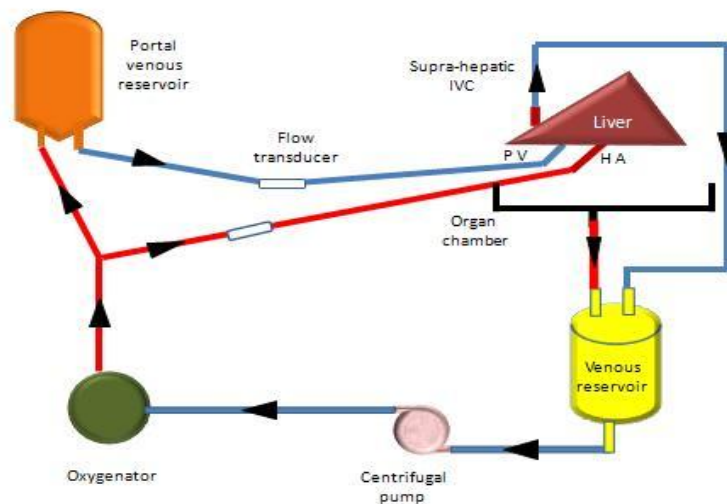

Fig. 1. Schematic drawing of the circuit for the *ex-vivo* perfusion of the liver

2.4 Microwave Ablation

In each liver, MWA lesions were created one hour after liver perfusion to make sure all physiological parameters have settled. The microwaves were generated by a Microsulis Tissue Ablation Sulis TMV Generator (Microsulis Ltd., Denmead, Hampshire, UK) at a frequency 2.45 GHz and delivered via the Accu5i applicator (Microsulis Ltd., Denmead, Hampshire, UK) which has a shaft diameter of (9 mm) and a biocompatible non-stick coating.

The applicator was inserted to 2 cm beneath the surface of the liver in all applications to achieve a consistent shape throughout the study. Nine lesions were created at power 50W, 70W and 90 W (three lesions for every power). Each lesion was created for two minutes (Fig. 2).

2.5 Liver Scanning

Baseline liver images were taken without and with contrast agents CA. After MWA, the liver was again scanned without and with CA. All images and cine loops were saved on a LOGIQ 9 US machine (GE Healthcare, Chalfont St Giles, UK). The CA (Sonovue, Bracco, Milano, Italy) consisted of phospholipid-stabilized MBs containing Sulphur Hexafluoride gas with a diameter of less than 8 µm (mean 2.5 µm) reconstituted with 5 ml of 0.9% normal saline solution. The CA was injected in the hepatic artery (HA) valve and flushed with 5ml normal saline.

2.6 Quantification of MBs in the Ablated Zone

The US machine was equipped with a specific contrast software to create "wash-in"/"wash-out" curves, a measure of the contrast acquisition and removal in a particular scanned area, evidenced during the imaging acquisition and processing. The software provided real-time images with and without the presence of contrast, and the intensity of the acoustic signal was assessed on the video recording extracted every 5s following injection. Standardized 12- to 18-mm regions of interest were chosen for analysis from hyperechoic, hypoechoic, and anechoic areas. The parameters which were evaluated from the time–intensity curves included "time to peak" (time elapsed from the start of the scan to the maximum intensity of the medium contrast in a defined region, evaluating how quickly the medium contrast peaks in that region),

"maximum gradient" (maximum difference between the lowest and highest values recorded of the medium contrast intensity from the start to the end of the scan, evaluating the net increase of contrast reaching that region), and the "area under the curve" (the area under the actual time–intensity curve of the medium contrast, a measure of the total amount of contrast reaching the area over the scan).

2.7 Lesion Analysis

The lesions were sliced and the dimensions (long-axis "LA" and short-axis "SA") of the whole lesions were measured on morphology, grey-scale US, CEUS and then compared. Wedge biopsies were taken from the lesion for histology. All biopsies were saved in Formalin and then assessed with Haematoxilin-Eosin (HE) stain. All data were entered into an Excel database. Numerical data reported as mean (M) +/_ standard deviation (SD). Analysis of data was performed with ANOVA test. A (P value of <0.05) was considered significant.

3. RESULTS

3.1 Grey-scale US

All baseline images showed homogenous enhancement of liver tissue. The ablations were reported as one hypoechoic area compared to the normal isoechoic surrounding liver parenchyma (Fig. 3, "left panel"). For powers 50 W, 70 W and 90 W, the mean values for the LA dimensions were (25.8 +/_ 1 mm), (28.9 +/_ 2.8 mm), (34.6 +/_ 2 mm) respectively, and for the SA were (25.2 +/_ 0.8 mm), (28.1 +/_ 2.2 mm), (26.3 +/_ 2.7 mm) respectively. There was a significant difference in the LA between power 50W and 90W (P 0.05) (Fig. 4). There was no difference in the SA among the powers.

3.2 CEUS

All baseline images showed homogenous enhancement of the liver tissue with the CA. The ablations were reported as anechoic with well-demarcated borders separating them from the contrast-enhanced liver parenchyma in the arterial and venous phase (Fig. 3 "right panel"). The ablated areas did not show any contrast in them apart from the probe insertion site. The LA mean values for powers 50 W, 70 W and 90 W were (26.2 +/_ 1.1 mm), (30.7 +/_ 2.2 mm), (44 +/_ 4 mm), and for the SA were (27.9 +/_ 06 mm), (30.8 +/_ 1.6 mm), (31.5 +/_ 1.8 mm),

respectively. There was a significant difference in the LA between powers 70 W and 90 W (P 0.015) and a significant difference in the long-axis between powers 50 W and 90 W (P 0.001) (Fig. 5). There was no difference in the SA dimensions among the three powers.
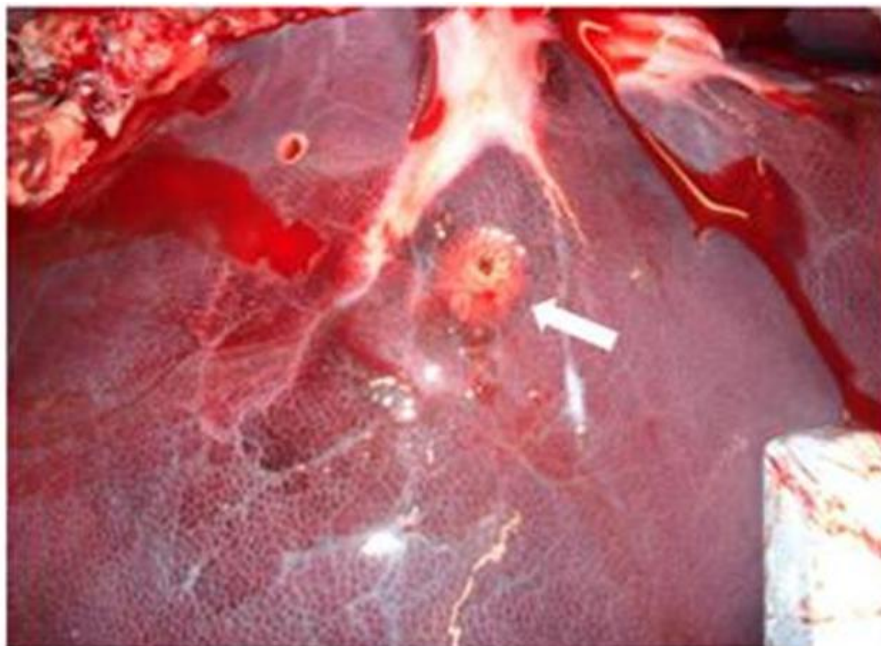

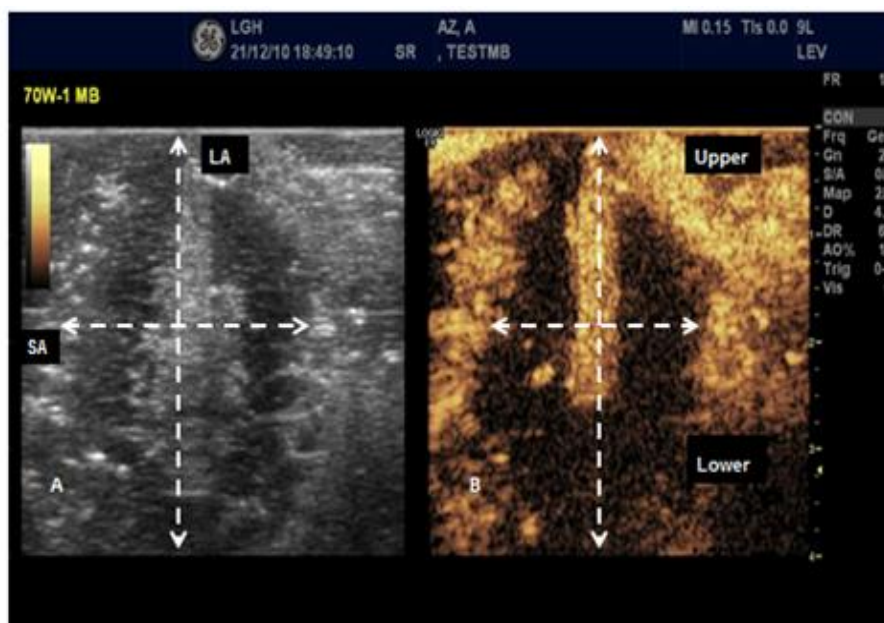**Fig. 2. Example of the created lesions in the porcine liver**

Fig. 3. Hypoechoic lesions with different powers on grey-scale ultrasound (left panel-A) and with CEUS (right panel-B), Notice the enhancement of the probe insertion site with CA (white arrow), LA (long axis), SA (short axis)

3.3 Histology

3.3.1 Gross morphology

Each lesion consisted of three zones; central charring "black" around the probe insertion site, surrounded by a white pale zone, and then a red-purple perinecrotic zone separating it from the normal looking liver tissue (Fig. 6). The zones were all spherical in shape. The whole diameter of the lesion was taken including all zones (Fig. 7). The LA mean values for power 50 W, 70 W and 90W were (31.7 +/- 3.1 mm), (35.18 +/_ 1.1 mm), (43.3 +/_ 3.3 mm) respectively, and for the SA were (28.9 +/_ 1.6 mm), (30.3 +/_ 2.3 mm), (32.18 +/_2.1 mm), respectively. There was a significant difference in the long-axis diameter between power 50 W and 90 W (P 0.034) (Fig. 8), but no difference in the short axis diameter. The mean values for the perinecrotic zones were (2.3 +/_ 0.09 m), (2.9 +/_ 0.2 mm), (2.9 +/_ 0.3 mm) respectively, with no difference.
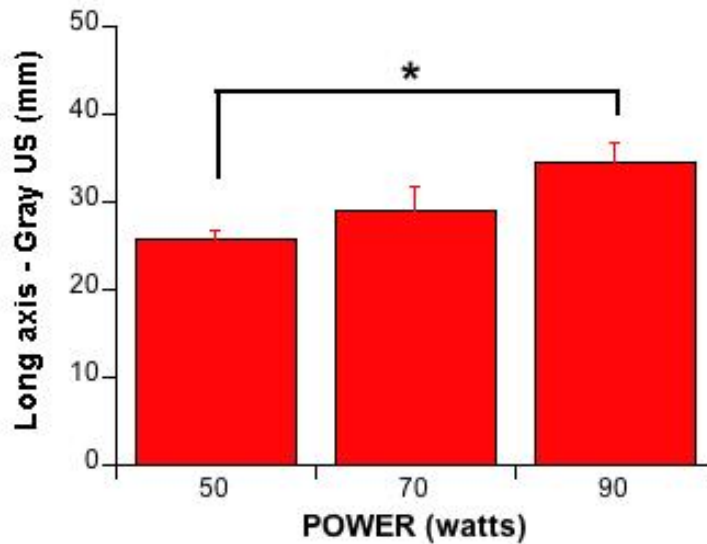

Fig. 4. Comparison of the lesion's long-axis on grey-scale ultrasound among the three different powers showing the significant difference between power 50W and 90W, P = 0.05
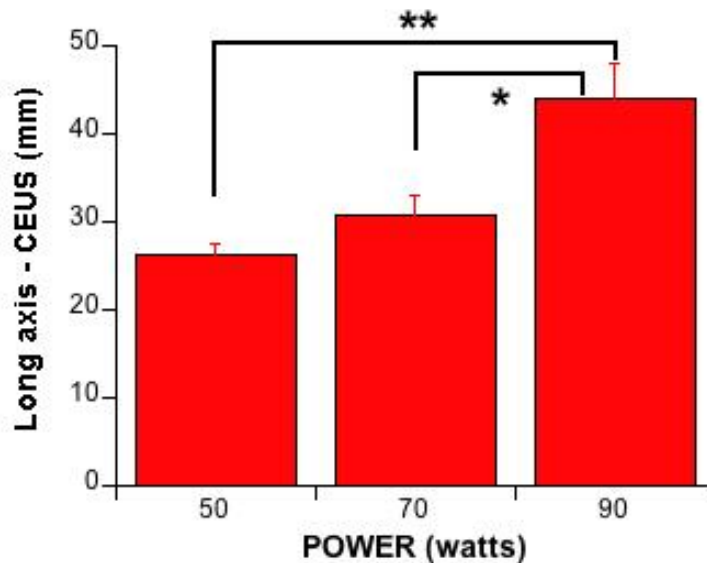

Fig. 5. Comparison of the lesion's long axis among the three different powers on CEUS showing significant difference between power 70W and 90W (P = 0.015), and between power 50W and 90W (P = 0.0015)
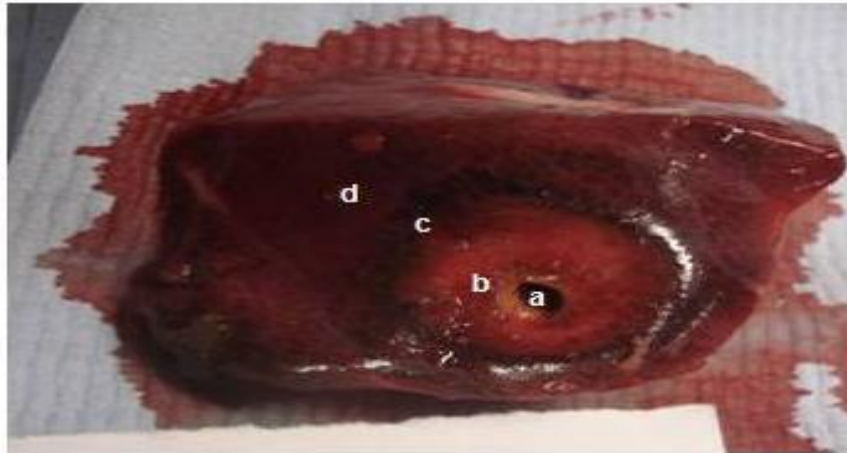
Fig. 6. A microwave ablation lesion sample showing the different zones; probe insertion site "a", necrotic zone "b", perinecrotic zone "c", and normal liver tissue "d"
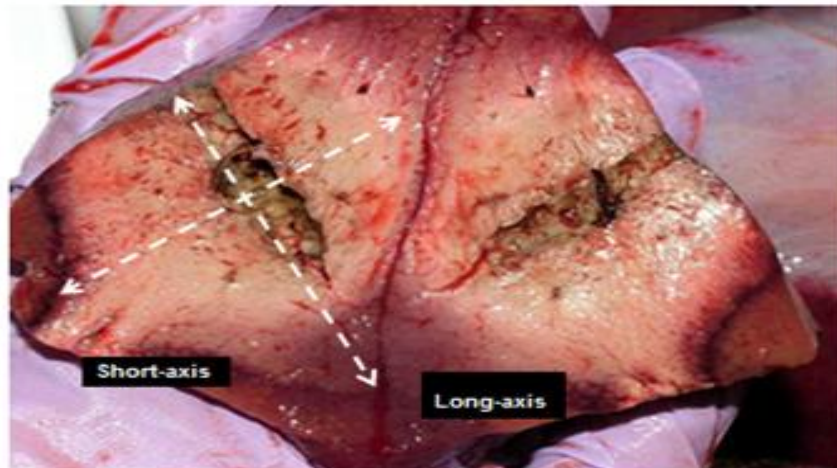

Fig. 7. Measurements of a lesion dimensions on morphology
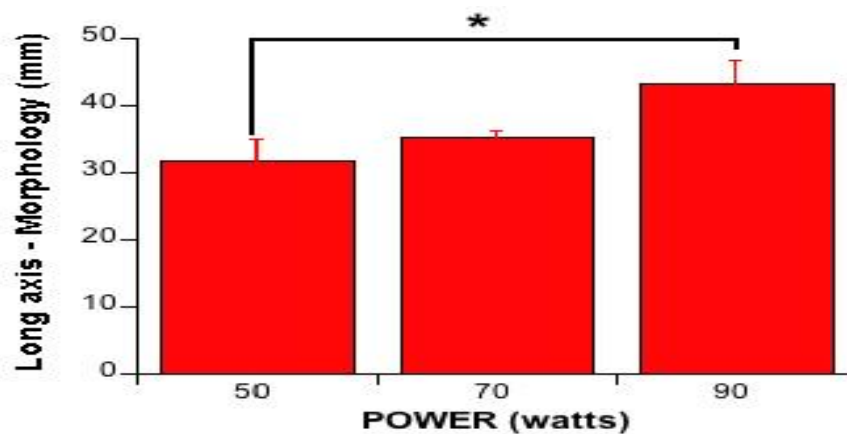

Fig. 8. Comparison of the lesion's long-axis on morphology among the three powers showing a significant difference between power 50W and 90W "P =0.034"

3.3.2 Microscopy

Thermal damage was shown around the probe insertion site with signs of central coagulative necrosis with unrecognizable cell boundaries and collapsed collagen fibres consistent with the white zone (Fig. 9). This zone was surrounded by a TZ with signs of vacoulisation of hepatocytes, sinusoidal dilatation and haemorrhagic extravasation of red blood cells from the sinusoids into the liver parenchyma, consistent with the red-purple perinecrotic zone on macroscopy (Fig. 10). The mean values for the TZ width for powers 50W, 70W and 90W were (0.4 +/_ 0.02 mm), (0.5 +/_ 0.06 mm), (0.6 +/_ 0.02 mm), respectively. There was a significant difference in the dimensions between powers 50 W and 90 W (P = 0.015) (Fig. 11).
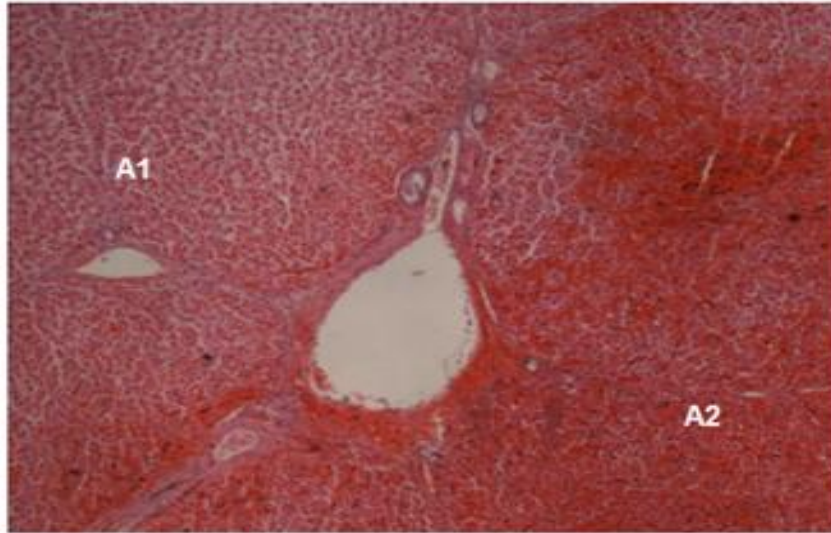
Fig. 9. Histological examination of the ablated zone showing central coagulative necrosis "A1" with unrecognizable cell boundaries and collapsed collagen fibres "X 40". Transitional zone "A2"
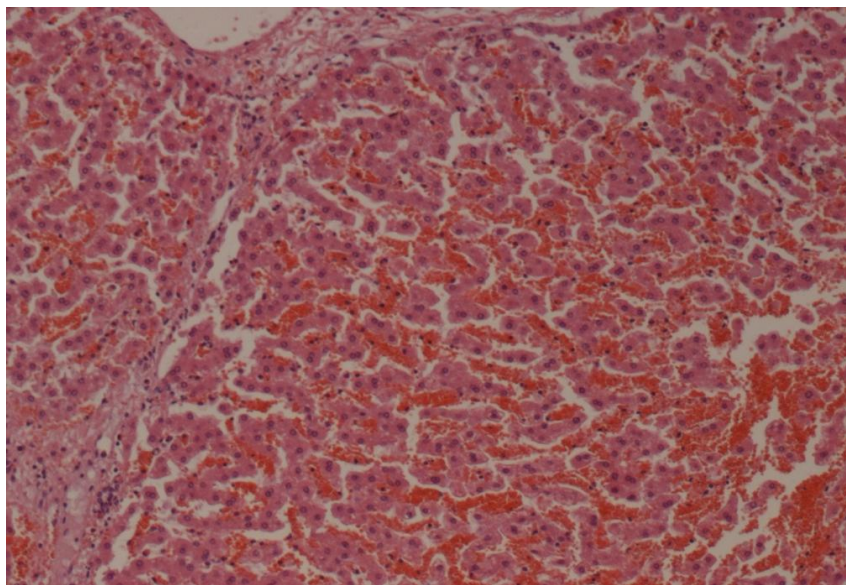
Fig. 10. Histological examination of the transitional zone showing vacoulisation of hepatocytes, sinusoidal dilatation and haemorrhagic extravasation of red blood cells from the sinusoids into the liver parenchyma "X 100"

3.4 Data Comparison

There was a significant difference between the LA of the ablations on morphology, grey-scale US and CEUS (P=0.0001). There was also a significant difference in the lesion size between powers (P= 0.0064) (Fig. 12). There was no difference in the SA for the ablations on morphology, grey-scale US and CEUS, but there was a significant difference in the lesion size between powers (Fig. 13).

3.5 Quantification of the MBs in the Ablated Area

The whole ablated areas (centre and periphery) did not show signs of enhancement with CA during the "Wash in" and "Wash out" phases and all curves were flat, corresponding to the central necrotic and perinecrotic zones (due to stasis), while the healthy perfused liver tissue around the ablations showed homogeneous enhancement (Fig. 14).
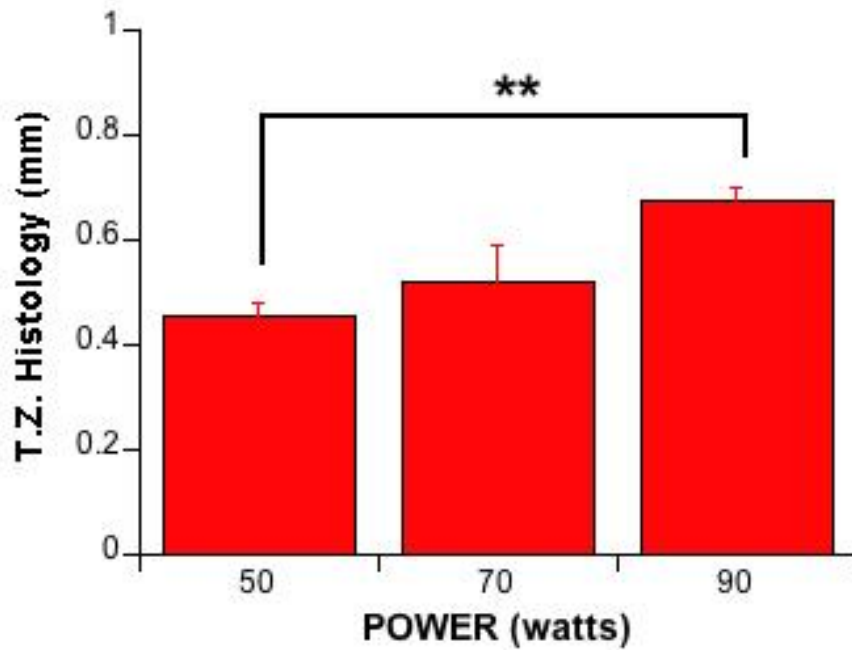

Fig. 11. Comparison of the transitional zone width on histology among the three different powers a significant difference in the dimensions between powers 50 W and 90 W "P = 0.015"
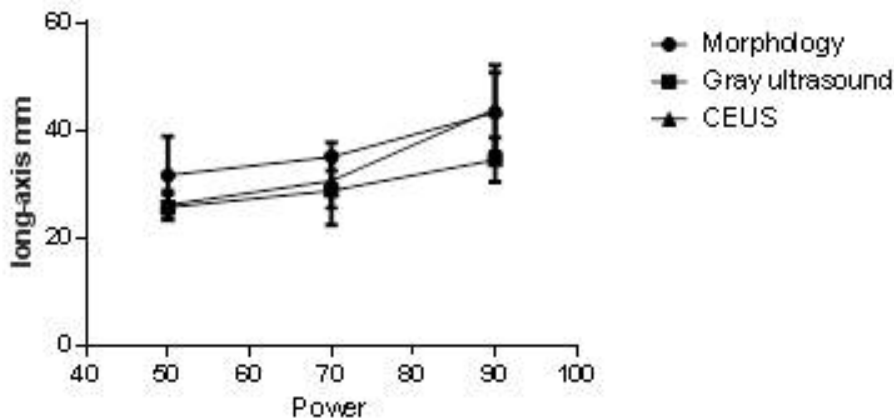
Fig. 12. Data analysis "ANOVA test" showing the correlation in the long-axis of the lesion between morphology, grey-scale US
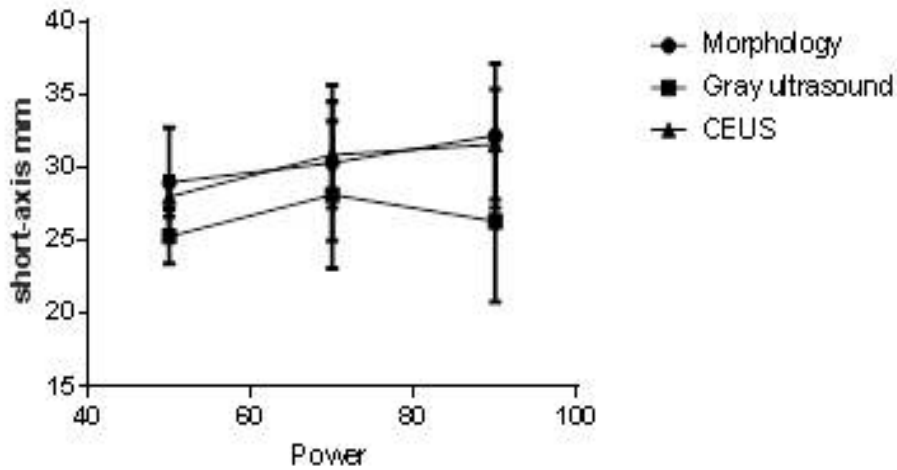
Fig. 13. Data analysis "ANOVA" test) showing the correlation in the short-axis of the lesion between morphology, grey-scale US and CEUS showing no difference. There is a significant difference in the lesion size among the powers "P = 0.03"
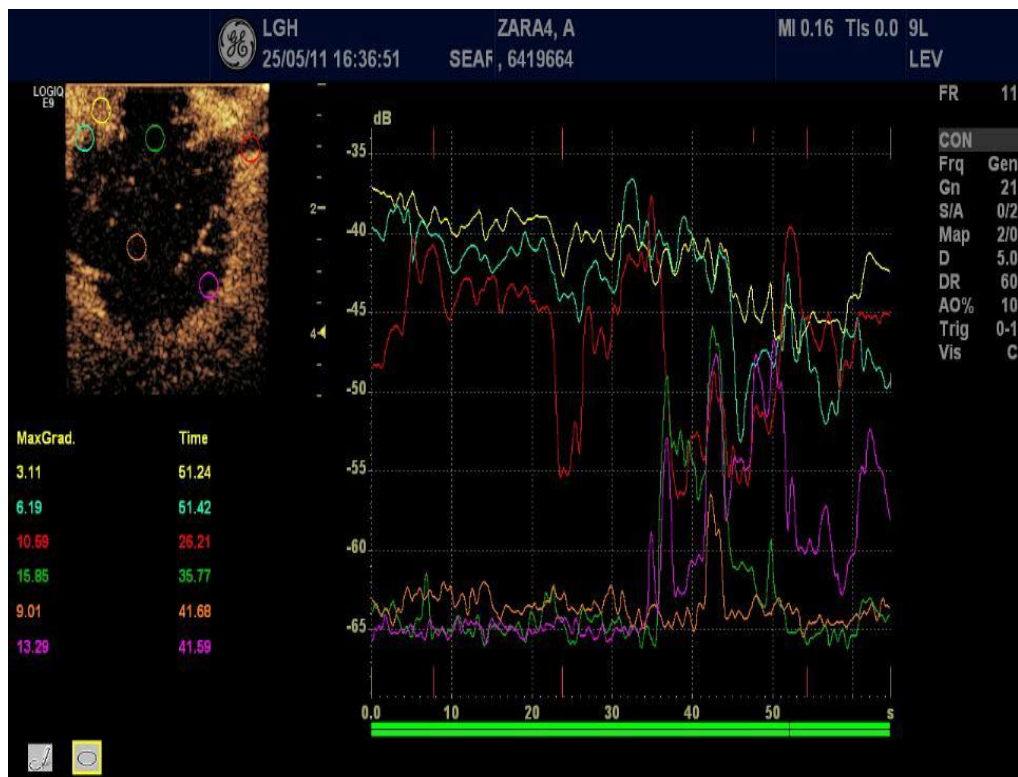
Fig. 14. Example of the quantification of the CA in the ablated area showing different time–intensity curves. The flat (orange, green and purple) curves correspond to the necrotic area with no perfusion. The "yellow, blue and red" curves correspond to the perfused normal liver tissue during "Wash in" and "Wash out" The coloured circles in the left upper panel represent the regions of interest "12–18 mm" where data were sampled during the contrast administration "colour figure online"

4. DISCUSSION

Due to its flexible approach (laparoscopic, percutaneous, with open surgery), MWA has become of the new trends for treating liver cancer [6,24,25]. Its advantages over other thermal ablative techniques include higher intratumoural temperatures, faster ablation times, improved heating of cystic lesions, less procedural pain as it does not require the placement of grounding pads, and is less susceptible to heat sink which means consistency in the size and the shape of the ablated zone [1,8,17].

These advantages have made MWA useful for treating primary liver cancer and secondary metastases. Primary liver cancer is the sixth cancer worldwide with hepatocellular carcinoma (HCC) accounting for 70%-90% of the total incidence [26,27]. MWA can be performed under CT, MRI or US guidance. US-guided MWA is more convenient as it allows scanning body in different positions, does not involve radiation and is less costly [28-30]. On the other hand, US does not always show tumour target because of its texture or even differentiate residual tumour from the treated area after ablation [13,31,32]. The recommended guideline of ablation is to destroy cancerous lesions with a normal tissue circumferential safety margin of 5 mm to 10 mm to make sure that the whole lesion is treated [10,33]. After thermal ablation of a tumour, a hyperaemic rim appears which surrounds the ablated area [11,12]. The rim is not visible on grey-scale US, but contrast CT, MRI and CEUS show this rim as uniform, homogeneous, larger than the initial lesion in benign tumours, and irregular, with a size similar to the initial cancerous lesion if the ablation is not complete [10,13]. Irregular borders mean that residual cancer might still exists as some cancer cells escape heat causing local recurrence. By definition, residual tumour is the hyperenhanced area in the ablated area in the arterial phase, with portal and late wash-out [13]. This means multiple reinsertions of the probe may be required to achieve complete destruction of the lesion, prolonging operation time, risking exposure to radiation or even causing unnecessary damage to normal tissues around the lesion [34]. Grey-scale US lacks the capability of showing targets clearly during treatment because of the generated steam from the ablation which obscures the view [33,35]. The steam creates a problem with differentiating healthy from necrotic tissue "especially in patients with borderline liver volume and function", identifying lesions in difficult anatomic positions which can only be treated with a probe, or even inserting the probe for overlapping burns [8,10,33].

CEUS allows imaging of liver tissues in real-time (arterial phase, venous phase and parenchymal phase [10,36]. It also guides viable tissue, avoids necrotic areas, evaluates the therapeutic effect immediately post-procedure, and possible reintervention in case of partial response [13]. The superiority of the CEUS in the detection of focal liver lesions outweighs the limitation of cost when compared to grey-scale US. Contrast agent needs special software installed on US machine for it to be detected. Furthermore, the cost of the CA itself should also be taken into consideration. In their study on 25 patients who underwent ablation of hepatic tumours, Andreano and colleagues [11] suggested including the enhanced peripheral rim to achieve complete ablation of tumours. They assessed the lesions with CEUS and found a highly significant difference (P<0.0001) in the lesion size before and during the arterial phase of contrast enhancement. Meloni et al. [10] assessed the diagnostic accuracy of CEUS immediately after ablation, after 24-h, and compared it with the diagnostic accuracy of CT after 24-h and then with both imaging methods after 3 months. He evaluated 55 tumours in the liver (37 treated with radiofrequency ablation "RFA" and 18 with MWA) in 53 patients and concluded that the immediate postprocedural CEUS was comparable to 24-h CEUS and CT in terms of detecting residual disease. In a pilot study on twenty one patients with known hepatic lesions, contrast-enhanced intraoperative ultrasound (CE-IOUS) detected additional 4 lesions and helped change management in three patients [22].

In this study, although CEUS did show better demarcation of the lesions in the images when compared with grey-scale ultrasound, when ANOVA test was performed, there was a significant difference in the long-axis among morphology, grey-ultrasound, and CEUS. The same test did not show a significant difference in the short-axis when all evaluation modalities were compared. These results suggest that CEUS in this study is not superior to grey-scale US or morphology in the assessment of the lesion size. Lesion dimensions did increase with increasing powers, but this is not a new discovery, and the results match what has been published by other investigators. Yang et al.

Hines-Peralta et al. and Kuang et al. showed a sigmoid curve correlation between increasing power and the duration of treatment and the ablation size in ex vivo models [37-39].

In their review of the histological changes post MWA in porcine livers, Gravante G et al. [15] concluded the microscopic changes in three different zones. First; a central zone of coagulative necrosis with loss of cell membranes, amorphous cytoplasm, pyknotic nuclei, loss of nucleoli and reduction in the intercellular spaces. Second; an intermediate zone of swollen and dead hepatocytes, undefined cell walls, granular debris and erythrocyte remnants in the sinusoids, and indistinct Kupffer cells with no nuclei and separated from liver cell plates. Third: A peripheral haemorrhagic zone consisting of intact liver cell plates, sharply defined cell wall, normal nuclei, oedematous sinusoids with intact erythrocytes, normal outline of the lobules and normal septal fibrocollagenous tissue. Our study also confirmed similar results. To our knowledge, no study has correlated the width of the transitional zone with increasing ablation power or with CEUS in an ex vivo liver model yet. In our experiment, microscopic examination of the lesion did show an increase in in the width of the transitional zone with increasing power, but the results did not correlate with the width of the perinecrotic red zone on morphology. This means that histology is the only way to properly evaluate the transitional zone, while morphology failed to do so because of the inflammation which masks the picture. This was also obvious with the CEUS which showed a central hypoechoic zone surrounded by the enhanced liver with normal blood flow. The perinecrotic zone was not visible due to stasis which is caused by the inflammatory process.

5. LIMITATIONS OF THE STUDY

Our experiment had few limitations. First: the small sample of experiments. Second: the short life span for the ex vivo model which could be kept live for a maximum of six hours only in order to achieve convincing results. Third: the absence of other interacting organs which have an important effect on liver physiology which influences data.

6. CONCLUSION

Our results match the previous studies which showed similar correlation between power and

lesion size, and histological characteristics of the ablated zones. There is better demarcation of the ablated zone border with CEUS when compared with grey-scale US, an advantage that could be very useful if it was to be implemented in clinical practice to immediately aid lesion evaluation post MWA therapy. On the other hand, CEUS does not reflect the actual size of the lesion when compared with grey-scale US or morphology. Furthermore, histology remains the only way to reflect the exact width of the transitional zone. Another advantage of the study is that all experiments were performed on an ex vivo liver model without the need for live animals. Further similar studies are still required to confirm and support our findings.

CONSENT

It is no applicable.

INSTITUTIONAL ETHICAL APPROVAL

All authors hereby declare that "Principles of laboratory animal care" (NIH publication No. 85-23, revised 1985) were followed, as well as specific national laws where applicable. All experiments have been examined and approved by the appropriate ethics committee".

ACKNOWLEDGEMENTS

COMPETING INTERESTS

Authors have declared that no competing interests exist.

REFERENCES

1. Simon CJ, Dupuy DE, Mayo-Smith WW. Microwave ablation: Principles and applications. Radiographics: A Review Publication of the Radiological Society of North America, Inc. 2005;25(Suppl1):69-83.
2. Byrd JF, Agee N, McKillop IH, Sindram D, Martinie JB, Iannitti DA. Colour doppler ultrasonography provides real-time microwave field visualisation in an *ex vivo* porcine model. HPB: The official Journal of the International Hepato Pancreato Biliary Association. 2011;13(6):400-403.

3.   Lubner MG, Brace CL, Hinshaw JL, Lee FT. Microwave tumor ablation: mechanism of action, clinical results, and devices. Journal of vascular and interventional radiology: JVIR. 2010;21(8Suppl):192-203.

4.   Umehara H, Seki T, Inokuchi R, Tamai T, Kawamura R, Asayama T, et al. Microwave coagulation using a perfusion microwave electrode: Preliminary experimental study using *ex vivo* and *in vivo* liver. Experimental and therapeutic medicine. 2012;3(2):214-220.

5.   Lubner MG, Hinshaw JL, Andreano A, Sampson L, Lee FT, Brace CL. High-powered microwave ablation with a small-gauge, gas-cooled antenna: Initial *ex vivo* and in vivo results. Journal of vascular and interventional radiology: JVIR. 2012;23(3): 405-411.

6.   Nouso K, Shiraga K, Uematsu S, Okamoto R, Harada R, Takayama S, et al. Prediction of the ablated area by the spread of microbubbles during radiofrequency ablation of hepatocellular carcinoma. Liver international. Official Journal of the International Association for the Study of the Liver. 2005;25(5):967-972.

7.   Swift B, Strickland A, West K, Clegg P, Cronin N, Lloyd D. The histological features of microwave coagulation therapy: An assessment of a new applicator design. International Journal of Experimental Pathology. 2003;84(1):17-30.

8.   Jones RP, Kitteringham NR, Terlizzo M, Hancock, C, Dunne D, Fenwick S, et al. Microwave ablation of *ex vivo* human liver and colorectal liver metastases with a novel 14.5 GHz generator. International journal of hyperthermia: The Official Journal of European Society for Hyperthermic Oncology, North American Hyperthermia Group. 2012;28(1):43-54.

9.   Vogt FM, Antoch G, Veit P, Freudenberg, Blechschmid LS, Diersch NO, et al. Morphologic and functional changes in nontumorous liver tissue after radiofrequency ablation in an *in vivo* model: comparison of 18F-FDG PET/CT, MRI, ultrasound, and CT. Journal of nuclear medicine: Official publication, Society of Nuclear Medicine. 2007;48(11): 1836-1844.

10.   Meloni MF, Andreano A, Franza E, Passamonti M, Lazzaroni S. Contrast enhanced ultrasound: Should it play a role in immediate evaluation of liver tumors following thermal ablation? European Journal of Radiology. 2012;81(8):e897-e902.

11.   Andreano A, Meneghel E, Bovo G, Ippolito D, Salvioni A, Filice C, et al. Contrast-enhanced ultrasound in planning thermal ablation of liver metastases: Should the hypervascular halo be included in the ablation volume? Journal of Ultrasound. 2010;13(4):158-163.

12.   Marin HL, Furthe E, Olthoff K, Shaked A, Soulen MC. Histopathologic outcome of neoadjuvant image-guided therapy of hepatocellular carcinoma. Journal of gastrointestinal and liver diseases: JGLD. 2009;18(2):169-176.

13.   Torzilli G, Olivari N, Moroni E, Del Fabbro D, Gambetti A, Leoni E, et al. Contrast-enhanced intraoperative ultrasonography in surgery for hepatocellular carcinoma in cirrhosis. Liver transplantation: Official Publication of the American Association for the Study of Liver Diseases and the International Liver Transplantation Society. 2004;10(2Suppl1):S34-S38.

14.   Bertram JM, Yang D, Converse MC, Webster JG, Mahvi DM. Antenna design for microwave hepatic ablation using an axisymmetric electromagnetic model. Biomedical engineering online. 2006;5:15.

15.   Gravante G, Ong SL, Metcalfe MS, Strickland A, Dennison AR, Lloyd DM. Hepatic microwave ablation: A review of the histological changes following thermal damage. Liver international: Official Journal of the International Association for the Study of the Liver. 2008;28(7):911-921.

16.   Zhou W, Liang M, Pan H, Liu X, Jiang Y, Wang Y, et al. Comparison of ablation zones among different tissues using 2450-MHz cooled-shaft microwave antenna: results in *ex vivo* porcine models. PloS one. 2013;8(8):e71873.

17.   Awad MM, Devgan L, Kamel IR, Torbensen M, Choti MA. Microwave ablation in a hepatic porcine model: correlation of CT and histopathologic findings. HPB: The Official Journal of The International Hepato Pancreato Biliary Association. 2007;9(5):357-362.

18.   Matsukawa T, Yamashita AY, Arakawa A, Nishiharu T, Urata J, Murakami R, et al. Percutaneous microwave coagulation therapy in liver tumors. A 3-year experience. Acta radiologica. 1997;38(3): 410-415.

19.   Kato T, Suto Y, Hamazoe R. Effects of microwave tissue coagulation on the livers

of normal rabbits: A comparison of findings of image analysis and histopathological examination. The British Journal of Radiology. 1996;69(822):515-521.

20. Hyodoh H, Furuse M, Kawamoto C, Isoda N, Ido K, Saito K. Microwave coagulation therapy: *ex vivo* comparison of MR imaging and histopathology. Journal of Magnetic Resonance Imaging: JMRI. 2000; 11(2):168-173.

21. Strickland AD, Clegg PJ, Cronin NJ, Swift B, Festing M, West K, et al. Experimental study of large-volume microwave ablation in the liver. The British Journal of Surgery. 2002;89(8):1003-1007.

22. Shah AJ, Callaway M, Thomas MG, Fich-Jones MD. Contrast-enhanced intraoperative ultrasound improves detection of liver metastases during surgery for primary colorectal cancer. HPB: The Official Journal of The International Hepato Pancreato Biliary Association. 2010;12(3):181-187.

23. Ong SL, Gravate G, Metcalfe MS, Dennison AR. History, ethics, advantages and limitations of experimental models for hepatic ablation. World Journal of Gastroenterology: WJG. 2013;19(2):147-154.

24. Jagad RB, Koshariya M, Kawamoto J, Papastratis P, Kefalourous H, Patris V, et al. Laparoscopic microwave ablation of liver tumors: Our Experience. Hepato-Gastroenterology. 2008;55(81):27-32.

25. Brace CL, Hinshawi JL, Lubner MG. Thermal ablation for the treatment of abdominal tumors. Journal of Visualized Experiments: JoVE. 2011;49.

26. Van Meer S, De Man RA, Siersema PD, Van Erpecum KJ. Surveillance for hepatocellular carcinoma in chronic liver disease: evidence and controversies. World Journal of Gastroenterology: WJG. 2013;19(40):6744-6756.

27. Liang P, Yu J, Lu MD, Dong B, Yu X, Zhou X, et al. Practice guidelines for ultrasound-guided percutaneous microwave ablation for hepatic malignancy. World Journal of Gastroenterology: WJG. 2013;19(33): 5430-5438.

28. Ng KK, Poon RT, Lo CM, Yuen J, Tso W K, Fan ST. Analysis of recurrence pattern and its influence on survival outcome after radiofrequency ablation of hepatocellular carcinoma. Journal of Gastrointestinal Surgery: Official Journal of the Society for Surgery of the Alimentary Tract. 2008; 12(1):183-191.

29. Jensen JA. Medical ultrasound imaging. Progress in biophysics and molecular biology. 2007;93(1-3):153-65.

30. Ihnatsenk B, Boezaart AP. Ultrasound: Basic understanding and learning the language. International Journal of Shoulder Surgery. 2010;4(3):55-62.

31. Liu LN, Xu HX, Zhang YF, Xu JM. Hepatocellular carcinoma after ablation: The Imaging Follow-up Scheme. World Journal of Gastroenterology: WJG. 2013; 19(6):797-801.

32. Meloni MF, Goldberg SN, Livraghi T, Calliada F, Ricci P, Rossi M, et al. Hepatocellular carcinoma treated with radiofrequency ablation: Comparison of pulse inversion contrast-enhanced harmonic sonography, contrast-enhanced power Doppler sonography, and helical CT. AJR American Journal of Roentgenology. 2001;177(2):375-380.

33. McCarley J R, Soulen MC. Percutaneous ablation of hepatic tumors. Seminars in Interventional Radiology. 2010;27(3):255-260.

34. Clarke CN, Kuboki S, Tevar A, Lentsch A B, Edwards M. CXC chemokines play a critical role in liver injury, recovery, and regeneration. American Journal of Surgery. 2009;198(3):415-419.

35. Sparchez Z, Radu P, Anton O, Socaciu M, Badea R. Contrast enhanced ultrasound in assessing therapeutic response in ablative treatments of hepatocellular carcinoma. Journal of Gastrointestinal and Liver Diseases: JGLD. 2009;18(2):243-248.

36. Claudon M, Dietrich CF, Choi BI, Cosgrove D, Kudo M, Nolsoe C, et al. Guidelines and good clinical practice recommendations for Contrast Enhanced Ultrasound (CEUS) in the liver - update 2012: A WFUMB-EFSUMB initiative in cooperation with representatives of AFSUMB, AIUM, ASUM, FLAUS and ICUS. Ultrasound in Medicine & Biology. 2013;39(2):187-210.

37. Yang D, Bertram JM, Converse MC, O'Rourke AP, Webster JG, Hagness SC, et al. A floating sleeve antenna yields localized hepatic microwave ablation. IEEE Trans Biomed Eng. 2006;53:533–537.

38. Hines-Peralta AU, Pirani N, Clegg P, Cronin N, Ryan TP, Liu Z, et al. Microwave ablation: Results with a 2.45-GHz applicator in *ex vivo* bovine and in vivo porcine liver. Radiology. 2006;239:94–102.

39. Kuang M, Lu MD, Xie XY, Xu HX, Mo LQ, Liu GJ, et al. Liver cancer: Increased microwave delivery to ablation zone with cooled-shaft antenna – experimental and clinical studies. Radiology. 2007;242:914–924.

Peer-review history:
The peer review history for this paper can be accessed here:
http://www.sciencedomain.org/review-history.php?iid=1116&id=12&aid=9010